

Method for Determining AGN Accretion Phase in Field Galaxies

Miroslav Micic^{1*}, Nemanja Martinović¹, Manodeep Sinha²

¹ *Astronomical Observatory Belgrade*

² *Department of Physics & Astronomy, Vanderbilt University*

17 June 2016

ABSTRACT

Recent observations of AGN activity in massive galaxies ($\log M_*/M_\odot > 10.4$) show that: 1) at $z < 1$, AGN-hosting galaxies do not show enhanced merger signatures compared to normal galaxies; 2) also at $z < 1$, most AGNs are hosted by quiescent galaxies; and 3) at $z > 1$, percentage of AGNs in star forming galaxies increases and becomes comparable to AGN percentage in quiescent galaxies at $z \sim 2$. How can major mergers explain AGN activity in massive quiescent galaxies which have no merger features and no star formation to indicate recent galaxy merger? By matching merger events in a cosmological N-body simulation to the observed AGN incidence probability in the COSMOS survey, we show that major merger triggered AGN activity is consistent with the observations. By distinguishing between “peak” AGNs (recently merger triggered and hosted by star forming galaxies) and “faded” AGNs (merger triggered a long time ago and now residing in quiescent galaxies), we show that the AGN occupation fraction in star forming and quiescent galaxies simply follows the evolution of the galaxy merger rate. Since the galaxy merger rate drops dramatically at $z < 1$, the only AGNs left to be observed are the ones triggered by old mergers and are now in the declining phase of their nuclear activity, hosted by quiescent galaxies. As we go toward higher redshifts, the galaxy merger rate increases and the percentages of “peak” AGNs and “faded” AGNs become comparable.

Key words: Field AGN, supermassive black holes, dark matter halos, n-body simulations, COSMOS survey

1 INTRODUCTION

Galaxies residing outside of galaxy clusters are known as field galaxies. Their name implies a certain level of isolation; either in time between major interactions (~ 3 Gyr, Verdes-Montenegro et al. 2005), or through the surrounding environmental density (Dressler 1980).

The topic of this paper is AGN activity in field elliptical galaxies. These are massive ($\log M_*/M_\odot > 10.4$) galaxies, thought to be formed in gas rich major mergers of disk/spiral galaxies (Toomre 1977, White 1978, 1979, Gerhard 1981, Negroponte & White

1983, Barnes 1988, Hernquist 1989, Barnes & Hernquist 1996, Naab, Jesseit & Burkert 2006, Novak et al. 2012).

We focus on field AGNs because AGNs in massive elliptical galaxies are a field phenomena. Hwang et al. 2012 have studied a sample of almost a million SDSS galaxies. They found factor of three larger AGN fraction in the field compared to clusters. At higher redshift this increase is even more pronounced. Martini, Sivakoff & Mulchaey 2009 found an increase by factor of 8 at redshift $z = 1$.

Galaxy mergers are also a field phenomena. Low velocity dispersion in galaxy groups in the field leads to “slow encounters” (Binney & Tremaine 1987) which are necessary for the merger to occur. “Fast encoun-

* E-mail: micic@aob.rs

ters” are a characteristic of galaxy clusters. Energy input and dynamical friction scale as v^{-2} (Binney & Tremaine 1987) and do not lead to the merger but rather small perturbations which can fuel a low luminosity AGN (Lake, Katz & Moore 1998).

For a long time, major galaxy mergers have been a main mechanism for driving AGN activity (Sanders et al. 1988, Barnes & Hernquist 1996, Cavaliere & Vittorini 2000, Menci et al. 2004, Croton et al. 2006, Hopkins et al. 2006, Menci et al. 2008), both supermassive black hole (SMBH) accretion and star formation (Sanchez et al. 2004, Bohm et al. 2007, Schawinski et al. 2007, Silverman et al. 2008, Rafferty et al. 2011, Hopkins 2012). Observational evidence indicates post-merger features in galaxies hosting AGNs and quasars (Surace & Sanders 1999, Surace, Sanders & Evans 2000, Canalizo & Stockton 2000, 2001) lending credence to the theoretical picture of mergers as drivers of AGN activity. Fiore et al. 2012 found that theoretical models using galaxy interactions as AGN triggering mechanism are able to reproduce the high redshift ($z=[3, 7]$) AGN luminosity functions. The AGN fraction is higher in galaxy pairs (Silverman et al. 2011, Ellison et al. 2011, 2013).

This entire model was challenged recently (Gabor et al. 2009, Darg et al. 2010, Cisternas et al. 2011, Kocevski et al. 2012). Cisternas et al. 2011 found that 85 % of galaxies with AGNs do not show evidence of a previous merger at $z \leq 1$, which is consistent with the merger fraction of non-active galaxies.

Schawinski et al. 2011, Kocevski et al. 2012, and Simmons et al. 2012 showed that at $z \leq 3$ there is a high disk fraction in AGN hosts. Bohm et al. 2013 found that morphologies of the AGN hosts are similar to undisturbed galaxies. These observations suggested that secular evolution is responsible for SMBH growth, at least at low z . These could be internal processes such as bar-driven gas inflow (Kormendy and Kennicutt 2004), and stellar wind (Ciotti and Ostriker 2007, Ciotti, Ostriker & Proga 2010, Cen 2012). At that moment it seemed that secular evolution is the dominant mechanism behind the activity of low luminosity AGNs, while major mergers of galaxies are responsible for luminous AGNs.

Theoretical works also support this picture (Lapi et al. 2006, Hopkins, Kocevski & Bundy 2014). Hopkins, Kocevski & Bundy 2014 combined both merger and non-merger triggering of AGNs in semi-empirical model and found that secular (stochastic) fuelling is dominant in low luminosity AGNs which host SMBHs with mass $\leq 10^7 M_{\odot}$. For luminous AGNs hosting SMBHs with masses $\geq 10^8 M_{\odot}$ it accounts for just $\sim 10\%$ of black hole (BH) growth. This is consistent with the observations of post-starburst quasars (PSQs) which show that PSQs with lower luminosities reside in disk/spiral galaxies, while more luminous PSQs reside in early type galaxies (Cales et al. 2013).

However, Villforth et al. 2014 analysed the morphological properties of AGN host galaxies as a func-

tion of AGN and host galaxy luminosity and compared them to a carefully matched sample of control galaxies in the redshift range $z = [0.5, 0.8]$ and luminosity range $\log L_X [\text{erg/s}] = [41, 44.5]$. They found no increase in the prevalence of merger signatures with AGN luminosity and concluded that major mergers, even for higher luminosities, either play only a very minor role in the triggering of AGN or time delays are too long for merger features to remain visible. This conclusion questions galaxy mergers as drivers of any AGN activity.

In this paper we apply Shen 2009 SMBH growth model to the dark matter halo (DMH) merger trees in cosmological N-body simulation, in order to test if merger driven AGN activity is consistent with the activity of the observed AGNs in massive galaxies of COSMOS survey (Bongiorno et al. 2012).

In the first part of the paper we determine initial BH mass, and final (**true**) BH mass in the merger trees and then we use Shen 2009 AGN light curve model to grow initial BHs into final BHs. Next, we find our best fit model by matching it to the observed AGN luminosity function, active BHs mass function, duty cycle, and bias factor.

In the second part of the paper, we replace our best fit AGNs with COSMOS AGNs. We do this by using probability functions for galaxies to host AGNs in COSMOS, to determine probable AGN luminosities. We proceed with Monte Carlo procedure (40,000 realisations) where we replace peak luminosities in our best fit model with the COSMOS AGN luminosities. As the result, every postmerger halo has a 40,000 possible final BHs predicted by the model. Finally, we compare **predicted** BH masses to the **true** BH masses. We calculate the percentage of realisations when predicted SMBH mass is at least as large as the true SMBH mass. If that percentage is high, then the observed luminosity is the peak AGN luminosity. Otherwise, AGN is observed in the declining phase of its nuclear activity. This would place it in a massive, red, elliptical galaxy long after merger features can be detected, but its activity would still be consistent with merger driven model.

AGN hosts in COSMOS survey are mainly massive, red galaxies. Hence, their AGNs could potentially be merger driven, passed their peak activity during Green Valley, and in the declining Red Sequence phase. This interpretation would be consistent with the merger driven scenario for AGN activity and with the recent Schawinski et al. 2014 scheme for galaxy evolution.

We describe our method in section 2 and introduce two models based on initial BH mass function. In section 3, we present our best fit model. In section 4, we determine the phase of AGNs activity in COSMOS survey. We discuss the implications of our results, in section 5.

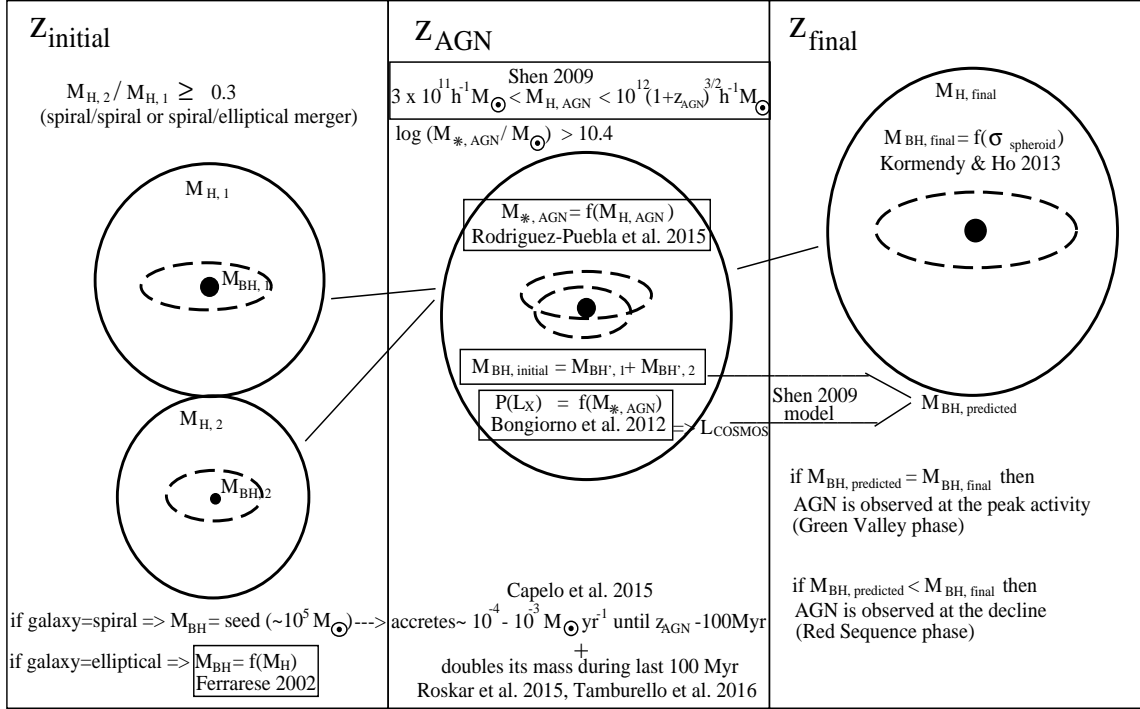


Figure 1. Graphical sketch showing the main steps of the methodology.

2 METHOD

The three major components in our model are: dark matter halo (DMH) merger trees from cosmological N-body simulation; Shen 2009 fit-by-observations semi-analytical model for major merger driven growth of SMBH; and Bongiorno et al. 2012 study of ~ 1700 AGNs and their host galaxies in COSMOS field survey.

The main idea is to track “field DMHs” undergoing major mergers in N-body cosmological simulation. Use Shen 2009 SMBH growth model and match it to the observations. Then we overlay our field with COSMOS field, match simulated galaxies to the observed COSMOS galaxies and assign COSMOS AGNs to them. Find if the observed AGNs are at their peak activity or in the declining phase.

Here is the outline of our model presented in figure 1.

(i) z_{initial} is the redshift of DMH merger. Halos touch and the smaller halo is inside the larger halo at all later times.

(ii) $M_{H,1}$ and $M_{H,2}$ are masses of merging halos at z_{initial} . We consider major mergers only, when mass ratio of merging halos is ≥ 0.3 .

(iii) If merging halo did not have major merger in its history, we assume that halo hosts a spiral galaxy. If halo had a major merger before, we assume it hosts an elliptical galaxy.

(iv) We seed spiral galaxies with pristine BHs ($\sim 10^5 - 10^6 M_{\odot}$) and elliptical galaxies with BHs from Ferrarese 2002 $M_{\text{BH}} - M_{\text{DMH}}$ relation. Masses of BHs hosted by merging halos are $M_{\text{BH},1}$ and $M_{\text{BH},2}$. Mergers of two elliptical galaxies do not trigger AGN activity (dry mergers).

(v) z_{AGN} is the redshift when smaller halo can not be identified anymore inside the larger one which means that the merger of DMHs has finished. We assume that mergers of their galaxies and black holes have finished too, and that accretion onto the new SMBH starts and enters AGN phase which has pre-peak and peak activity.

(vi) Even before central BHs ($M_{\text{BH},1}$ and $M_{\text{BH},2}$) form binary (BHB), they accrete at $\sim 10^{-3} - 10^{-4} M_{\odot} \text{ yr}^{-1}$ rate (Capelo et al. 2015), from z_{initial} at R_{vir} separation until BHB forms at $\sim \text{kpc}$ distance. This is the “pre-BHB accretion” phase. During the last ~ 100 Myr before BHs merge (at z_{AGN}), binary overcomes last couple of kpc and accretion increases to double the BH mass (Roskar et al. 2015, Tamburello et al. 2016). This is the “BHB accretion” phase. New masses of central BHs after these two accretion episodes are $M_{\text{BH}',1}$ and $M_{\text{BH}',2}$.

(vii) SMBH mass entering AGN phase at z_{AGN} , is then $M_{\text{BH},\text{initial}} = M_{\text{BH}',1} + M_{\text{BH}',2}$.

(viii) $M_{H,\text{AGN}}$ is the mass of DMH hosting an AGN at z_{AGN} . We adopt Shen 2009 model for AGN activity in field galaxies. This model implies halo

mass range $3 \times 10^{11} h^{-1} M_{\odot} < M_{H,AGN} < 10^{12} (1+z_{AGN})^{3/2} h^{-1} M_{\odot}$.

(ix) $M_{*,AGN}$ is the mass of the galaxy hosting an AGN at z_{AGN} . We consider only AGNs in massive galaxies ($\log(M_{*,AGN}/M_{\odot}) > 10.4$). Galaxy mass is obtained by using Rodriguez-Puebla et al. 2015 M_{*} - M_{DMH} relation.

(x) $P(L_X)$ is the probability of a galaxy to host an AGN of a given luminosity at z_{AGN} (Bongiorno et al. 2012). From it we obtain L_X and calculate bolometric AGN luminosity L_{COSMOS} .

(xi) $M_{BH,predicted}$ is the SMBH mass predicted by Shen 2009 model, when $M_{BH,initial}$ is the input parameter given in point (vii) and the peak luminosity is replaced by L_{COSMOS} .

(xii) z_{final} is the redshift of the postmerger halo $M_{H,final}$.

(xiii) $M_{BH,final}$ is the “true” mass of the postmerger BH, derived from $M_{BH} - \sigma_{sph}$ relation, calibrated to the local $M_{BH} - M_{DMH}$ relation (Ferrarese 2002).

(xiv) If the observed COSMOS AGN is at the peak activity, then $M_{BH,predicted}$ has to be at least as large as $M_{BH,final}$. Otherwise, AGN is in the declining phase of its nuclear activity.

In the following sections we describe simulation, data, and modelling in more details.

2.1 Cosmological N-body Simulation

Using GADGET2 (Springel, Yoshida & White 2001, Springel et al. 2005), we performed a high-resolution cosmological N-body simulation within a comoving periodic box with size of 130 Mpc^3 . WMAP5-like (Komatsu et al. 2009) cosmology was used ($\Omega_M = 0.25$, $\Omega_{\Lambda} = 0.75$, $n_s = 1$, $\sigma_8 = 0.8$ and $h = 0.7$) from $z = 599$ to $z = 0$ (84 snapshots). Initial conditions were computed with the 2LPT code (Crocce, Pueblas & Scoccimarro 2006). Simulation utilises 512^3 dark matter particles for a mass resolution of $1.14 \times 10^9 M_{\odot}$.

We generated halo catalogues using ROCKSTAR (Behroozi, Wechsler & Wu 2013). ROCKSTAR combines friends-of-friends (FOF), phase-space and spherical overdensity analysis in locating halos. Please see Behroozi, Wechsler & Wu 2013 for details on the ROCKSTAR algorithm. The merger tree was generated using Consistent Merger Tree (Behroozi et al. 2013), a software package that is complementary with the ROCKSTAR halo finder.

2.2 AGNs and galaxies in COSMOS survey

Bongiorno et al. (2012) have studied ~ 1700 AGNs in COSMOS field obtained by combining X-ray and optical spectroscopic selections. This is a highly homogeneous and representative sample of obscured and unobscured AGNs over a wide redshift range ($0 < z < 4$). By using Spectral Energy Distribution (SED) fitting procedure they have managed to separate host

galaxies properties including the total stellar mass of galaxies hosting AGNs. One of their results is the probability of a galaxy to host an AGN of a given luminosity ($P(L_X)$) as a function of stellar mass in three redshift bins: $[0.3 - 0.8]$, $[0.8 - 1.5]$, and $[1.5 - 2.5]$ (Figure 14 in their paper, from here on F14). They grouped AGNs in four logarithmic X-ray ($2 - 10 \text{ KeV}$) luminosity bins: $[42.8 - 43.5]$, $[43.5 - 44.0]$, $[44.0 - 44.5]$, and $[44.5 - 46.0]$ in erg/s units. They showed that for a fixed mass range, observed field galaxies are more likely to host less luminous AGNs. The probability that a field galaxy hosts an AGN decreases with increasing AGN luminosity.

2.3 SMBH growth model

We adopt Shen 2009 model for the hierarchical growth and evolution of SMBHs assuming that AGN activity is triggered in major mergers. This model uses a general form of light curve where BH first grows exponentially at constant luminosity Eddington ratio of $\lambda_0 = 3$ (Salpeter 1964) to L_{peak} at $t = t_{peak}$, and then the luminosity decays monotonically as a power-law (Yu & Lu 2008).

Shen 2009 uses a variety of observations. Model adopts Hopkins et al. 2007 compiled AGN bolometric luminosity function data for both unobscured and obscured SMBH growth. It also incorporates quasar clustering observations and the observed Eddington ratio distributions.

Model successfully reproduces the observed AGN luminosity function and both the observed redshift evolution and luminosity dependence of the linear bias of AGN clustering.

The input parameters for the Shen 2009 model are $M_{BH,initial}$ (mass of the BH entering AGN phase), L_{peak} (peak bolometric AGN luminosity), and $M_{BH,relic}$ (BH mass in the postmerger halo $M_{DMH,post}$ immediately after the AGN phase). To match our nomenclature, we have renamed $M_{BH,relic}$ to $M_{BH,final}$.

In our model, values for the first parameter come from the numerical simulation combined with the semi-analytical modelling (details in section 2.4).

We calculate $M_{BH,final}$ (details in section 2.6) from $M_{BH} - \sigma_{sph}$ relation (Kormendy & Ho 2013) where σ_{sph} is the velocity dispersion of the stellar spheroid. σ_{sph} is correlated with V_{vir} by a constant (Ferrarese 2002). We set this constant to a value which reproduces $z = 0$ Ferrarese 2002 $M_{BH} - M_{DMH}$ relation. Since $M_{BH} - \sigma$ relation is expected to be non-evolving, one can find M_{BH} in $M_{DMH,post}$ at any redshift. The outcome of this procedure is that the BH mass in high redshift halos, right after AGN phase, is overestimated. This is expected to occur as BH grows first, followed by postmerger halo growth through minor mergers and diffuse matter accretion. As we go toward lower redshifts, DMH growth catches up to SMBH growth to reproduce local Ferrarese relation

(Figure 6). Hence, we consider $M_{\text{BH,final}}$ to be the “true” final BH mass.

L_{peak} is the peak bolometric luminosity (details in section 2.7) in the Shen 2009 light curve model, set to the value which guarantees that the accretion onto $M_{\text{BH,initial}}$ produces $M_{\text{BH,final}}$. This is our ($L_{\text{peak,true}}$) best fit model which reproduces the observed AGN activity, luminosity function, duty cycle and bias factor.

After we demonstrate that our merger driven model reproduces observed AGN statistics, we test if the observed AGN activity in COSMOS survey corresponds to the peak or to the declining activity. Now, instead of $L_{\text{peak,true}}$, values for the peak luminosity (L_{COSMOS}) are retrieved from the probability for a galaxy to host an AGN of a given luminosity ($P(L_X)$) in COSMOS survey (details in section 2.8). We use this probability to seed galaxies with AGNs in 40,000 Monte Carlo realisations and grow SMBHs according to Shen 2009 model (details in section 2.9). The result is the probability that SMBHs grown in COSMOS AGNs match the true SMBHs grown in our best fit model.

2.4 Halos, galaxies, black holes: Initial values

We start by identifying major merger events in the merger trees of our cosmological N-body simulation. We define masses of merging halos as $M_{\text{H},1}$ and $M_{\text{H},2}$ at the time of the merger z_{initial} (figure 1). We also check if merging halos had major mergers previously. DMH without previous major merger is an ancient halo hosting disk/spiral galaxy with a large cold gas reservoir and the central BH that most likely formed through direct collapse of a gas cloud (Bromm & Loeb 2003, Begelman, Volonteri & Rees 2006, Begelman, Rossi & Armitage 2008). Latest observations (Mortlock et al. 2011) showed that BH seeds had to be massive ($\sim 10^5 - 10^6 M_{\odot}$) in order to grow $\sim 10^9 M_{\odot}$ BHs at redshift $z \sim 7$.

The initial mass function (IMF) and the mass range of the seed BHs are unknown. These BHs settle at the centres of disk/spiral galaxies but their masses do not correlate with any of the galaxy properties.

Growth of these initial BHs through accretion can occur even before they form a binary (BHB), during the early stages of the galaxy merger as galaxies go through subsequent pericentric passages (Capelo et al. 2015). As the major merger of galaxies proceeds, gravitational torques generate large-scale gas inflows that drive the gas down to sub-pc scale where it can be accreted by the BH. Hence, BHs grow in a modest amount even before they form a binary (pre-BHB accretion). Modelling of this growth is a subject of numerous numerical studies. However, limited resolution and disparate subgrid physics recipes led to a very different estimates of the BH accretion rates. Latest results (Hayward et al. 2014, Capelo et al. 2015) show that BH accretes at the rate $10^{-4} M_{\odot} \text{yr}^{-1} - 10^{-3} M_{\odot} \text{yr}^{-1}$ for ~ 1 Gyr before AGN phase.

After BH binary forms, accretion increases as BHs sink to overcome the last couple of kiloparsecs between them. During these last ~ 100 Myr before BH merger, BHs double their masses (Roskar et al. 2015, Tamburello et al. 2016). Assuming that Salpeter time is ~ 50 Myr, corresponding Eddington ratio is 0.35. This would mean that $10^6 M_{\odot}$ BH accretes at rate of $0.1 M_{\odot} \text{yr}^{-1}$, while $10^7 M_{\odot}$ BH accretes at the rate of $1 M_{\odot} \text{yr}^{-1}$ (over 100 Myr). This “BHB accretion” phase finishes with BH binary coalescence into a new BH which enters an AGN phase.

Unknown IMF for BH seeds, and rate of “pre-BHB accretion” are the main sources of uncertainty in our modelling. We overcome this issue by considering two models with the idea of constraining lower and upper end of possible initial BH mass. Our lower constraint model (M1) assumes log-normal IMF for BH seeds in the interval $\log(M_{\text{BH}}/M_{\odot}) = [4.5, 5.5]$ centered at $10^5 M_{\odot}$, and pre-BHB accretion with a rate of $\dot{m} = 10^{-4} M_{\odot} \text{yr}^{-1}$ from z_{initial} until z_{AGN} minus 100 Myr. For a higher constraint model M2 we set $\log(M_{\text{BH}}/M_{\odot}) = [5.0, 6.0]$ centred at $10^{5.5} M_{\odot}$ and $\dot{m} = 10^{-3} M_{\odot} \text{yr}^{-1}$. We seed DMHs with BHs by randomly choosing BH masses from these IMFs in Monte Carlo realisations. In the last 100 Myr before z_{AGN} , we double the BH mass (BHB accretion).

If DMH already had a major merger in its history, we assume it hosts an elliptical galaxy. BH at the centre of an elliptical galaxy scales with the properties of the stellar spheroid but also with the mass of the host DMH. We use Ferrarese 2002 $M_{\text{BH}} - M_{\text{DMH}}$ relation with $\pm 10\%$ scatter to seed elliptical galaxies with central BHs. Mergers of two elliptical galaxies do not trigger AGN activity (dry mergers). If an elliptical galaxy merges with a spiral, there is no pre-BHB or BHB accretion onto the BH at the centre of the elliptical galaxy.

Initial mass of the BHs in both halos ($M_{\text{BH},1}$ and $M_{\text{BH},2}$) combined with pre-BHB and BHB accretion (if galaxy is spiral) produces $M_{\text{BH}',1}$ and $M_{\text{BH}',2}$. Initial BH mass that enters AGN phase is then: $M_{\text{BH,initial}} = M_{\text{BH}',1} + M_{\text{BH}',2}$.

2.5 AGN phase

At z_{AGN} , initial BHs merge, form new BH ($M_{\text{BH,initial}}$). Mass of the DMH hosting an AGN is then $M_{\text{H,AGN}}$. Accretion onto $M_{\text{BH,initial}}$ starts first with the pre-peak phase at super Eddington rate ($\lambda = 3$) followed by the declining phase best described by Figure 2 in Shen 2009. We assume that AGN reaches its peak activity at z_{AGN} .

Note that in Shen 2009 model, AGN activity starts at the time when halos merge (not galaxies). Hence, the AGN activity in their model is pushed toward slightly higher redshifts. We find that the typical delay between halo merger and consecutive galaxy merger is $\Delta z = 0.2$ in redshift space and it does not impact overall results.

We adopt Shen 2009 model for AGN activity in field galaxies. We consider halos in mass range $3 \times 10^{11} h^{-1} M_{\odot} < M_{H,AGN} < 10^{12} (1+z_{AGN})^{3/2} h^{-1} M_{\odot}$. If halo mass is too small mass, AGN activity can not be triggered, while overly massive halos can not cool gas efficiently and BH growth halts (especially at low redshift) (Shen 2009). This excludes high density environments (e.g galaxy clusters) from our model and we are left with the AGN activity in the field. We do find that increasing the upper limit on host halo mass overpredicts the AGN luminosity functions at low redshift ($z \leq 1$).

Mass of the galaxy hosting an AGN is $M_{*,AGN}$. Since the topic of this paper is to examine merger driven AGN activity in massive galaxies in the field, we consider galaxies with $\log(M_{*,AGN}/M_{\odot}) > 10.4$. In lower mass galaxies, SMBHs are more likely to accrete through secular processes related to channeling of the gas through bars or disk instabilities.

Galaxy mass is obtained by using Rodriguez-Puebla et al. 2015 $M_* - M_{DMH}$ relation for early type (elliptical) galaxies (equations 17 and 18 and Figure 5 in their paper) with scatter $\sigma_r = \pm 0.136$ dex (equation 37 in Rodriguez-Puebla et al. 2015). Scatter determines galaxy mass in every Monte Carlo realisation.

2.6 Halos, galaxies, black holes: Final values

$M_{H,final}$ is the mass of the postmerger halo (immediately after the AGN phase) hosting final (relic) SMBH. We chose to define the time z_{final} to be ~ 100 Myr after AGN phase z_{AGN} , located in the first consecutive snapshot. However, mass of the postmerger halo changes insignificantly in more than one snapshot after z_{AGN} . In fact, our results do not change even when we use $M_{H,AGN}$ instead of $M_{H,final}$. This occurs because at the time of galaxy merger, new halo has already formed and for some time after the AGN phase it stays intact. Later, it continues growing by minor mergers and diffuse matter accretion. This implies that at first, mass of the final (relic) SMBH ($M_{BH,final}$) hosted by $M_{H,final}$ will be overestimated when compared to the local Ferrarese $M_{BH} - M_{DMH}$ relation. As $M_{H,final}$ grows in mass over time, $M_{BH,final} - M_{DMH,final}$ relation approaches Ferrarese relation.

Since $M_{BH} - \sigma_{sph}$ relation is expected to be non-evolving (Gaskell 2009, Shankar, Bernardi & Haimes 2009, Salviander, Shields & Bonning 2015, Shen et al. 2015), one can find $M_{BH,final}$ in $M_{DMH,final}$ at any redshift. First, one can rewrite equation (3) in Ferrarese 2002 as:

$$\frac{V_{vir}}{200 \text{ kms}^{-1}} = \left(\frac{M_{H,final}}{2.7 \times 10^{12} M_{\odot}} \right)^{1/3}, \quad (1)$$

Next, $\sigma_{sph} = C \times V_{vir}$. And from equation (7) in Kormendy & Ho 2013:

$$\frac{M_{BH,final}}{10^9 M_{\odot}} = 0.309 \left(\frac{\sigma_{sph}}{200 \text{ kms}^{-1}} \right)^{4.38}, \quad (2)$$

with scatter $\sigma = \pm 0.28$ dex.

We find that for $C = 0.77$, our $M_{BH,final} - M_{DMH,final}$ relation at $z=0$ matches local Ferrarese relation. As we go toward higher redshifts, Ferrarese relation evolves (figure 6) and $M_{BH,final}$ is overestimated while $M_{BH} - \sigma_{sph}$ does not evolve.

2.7 Finding Best Fit Model

Now that we have obtained $M_{BH,initial}$ and $M_{BH,final}$, we can calculate L_{peak} necessary to produce $M_{BH,final}$. As already mentioned in section 2.5, we use Shen 2009 AGN light curve with pre-peak exponential growth phase followed by post peak power-law decline. To calculate L_{peak} we rewrite equation (29) in Shen 2009:

$$L_{peak} = 3M_{BH,final} l_{Edd} \left(1 - \frac{2 \ln f}{3} \right)^{-1}, \quad (3)$$

and

$$f = \frac{3 l_{Edd} M_{BH,initial}}{L_{peak}} \quad (4)$$

where $l_{Edd} = 1.26 \times 10^{38} \text{ ergs}^{-1} M_{\odot}^{-1}$.

The descending phase is presented by equation 24 in Shen 2009:

$$L(L_{peak}, t) = L_{peak} \left(\frac{t}{t_{peak}} \right)^{-\alpha}, \quad (5)$$

where $\alpha = 2.5$. Luminosities of all AGNs in all galaxies and at all redshifts decrease three orders of magnitude from their peak luminosity in ~ 2 Gyr.

We use $M_{BH,initial}$, $M_{BH,final}$, and L_{peak} to calculate AGN luminosity function, active SMBH mass function, duty cycle, and bias factor. We compare these to the observed values. We find that both M1 and M2 models reproduce observations without any additional modelling or parameter fixing. We continue with M1 and M2 as our best fit models and later replace L_{peak} with L_{COSMOS} to find the AGN activity phase in COSMOS survey.

2.8 Matching COSMOS AGNs to $M_{*,AGN}$

For ~ 1700 AGNs in COSMOS field Bongiorno et al. 2012 presented probability of a galaxy of a certain mass to host an AGN of a given luminosity as a function of stellar mass in three redshift bins: [0.3 - 0.8], [0.8 - 1.5], and [1.5 - 2.5] (F14). They group AGNs in four X-ray (2 - 10 KeV) luminosity bins in logarithmic space: [42.8 - 43.5], [43.5 - 44.0], [44.0 - 44.5], and [44.5 - 46.0] (erg/s units). Masses of their AGN hosting galaxies are also separated in logarithmic bins: [9.0, 10.0], [10.0, 10.4], [10.4, 10.7], [10.7, 10.9], [10.9, 11.2] (M_{\odot} units).

How to pick a luminosity from F14 and assign it to our $M_{BH,initial}$? We do this by grouping our simulated galaxies at the moment their $M_{BH,initial}$ should start accreting.

We determine z_{AGN} , $M_{BH,initial}$, and $M_{*,AGN}$ for every merger in our simulation and group them into redshift bins:

$$\Delta z = [0.3 - 0.8; 0.8 - 1.5; 1.5 - 2.5], \quad (6)$$

and galaxy log-mass bins:

$$\Delta M_* = [10.4 - 10.7; 10.7 - 10.9; 10.9 - 11.2], \quad (7)$$

since we study AGNs in massive galaxies only.

In this manner we obtain nine Δz - ΔM_* intervals. The number of galaxies belonging to each Δz - ΔM_* interval is $N_{*,\text{AGN}}$. Next we match these Δz - ΔM_* intervals to the Δz - ΔM_* intervals in F14. According to F14, galaxies can host AGNs with luminosities in intervals:

$$\Delta L_X = [42.8-43.5; 43.5-44.0; 44.0-44.5; 44.5-46.0]. \quad (8)$$

So the BHs in $N_{*,\text{AGN}}$ simulated galaxies can be assigned with any of the luminosities from ΔL_X intervals. How these luminosities should be assigned is determined by the probability $P_{\text{AGN},i}$ (data points in F14) defined for every $\Delta L_{X,i}$.

$P_{\text{AGN},i}$ in F14 tells us that every galaxy in a specific Δz - ΔM_* interval is more likely to host low luminosity AGN.

Since the number of galaxies in each Δz - ΔM_* interval is $N_{*,\text{AGN}}$, then the number of times a luminosity should be drawn from each luminosity interval $\Delta L_{X,i}$ is:

$$N_{L,i} = \frac{P_{\text{AGN},i}}{\sum P_{\text{AGN},i}} \times N_{*,\text{AGN}}, \quad (9)$$

Largest $N_{L,i}$ is for the interval $\Delta L_{X,i}$ with smallest luminosities. The sum of $N_{L,i}$ is equal to $N_{*,\text{AGN}}$.

Next we randomly draw luminosities $N_{L,i}$ times from every corresponding $\Delta L_{X,i}$ and we randomly assign them to $N_{*,\text{AGN}}$ galaxies.

This is the first out of 40,000 Monte Carlo realisations where we draw luminosity values to be assigned to AGNs in each Δz - ΔM_* interval. Thus, for each $M_{*,\text{AGN}}$ we have a set of 40,000 COSMOS AGN luminosities. Since these are X-ray luminosities, we use equation 2) in Hopkins et al. 2007 to calculate bolometric luminosities. We address these luminosities as L_{COSMOS} . Next, we replace L_{peak} in our best fit model with L_{COSMOS} .

2.9 Modelling SMBH growth in COSMOS

With calculated $M_{\text{BH},\text{initial}}$ (mass of the BH entering AGN phase) and L_{COSMOS} (COSMOS bolometric AGN luminosity) we have two input parameters for Shen 2009 SMBH growth model. Evolution of AGN luminosities follows a universal general form of light curve with an initial exponential growth (pre-peak accretion) at constant Eddington ratio $\lambda = 3$ until it reaches L_{peak} , followed by a power-law decay. We replace L_{peak} with L_{COSMOS} .

Note that there are two sets of 40,000 $M_{\text{BH},\text{initial}}$ and L_{COSMOS} for each Δz - ΔM_* interval, obtained from Monte Carlo realisations in two models: M1 (lower range of seed BH masses) and M2 (upper range of seed BH masses).

After applying best fit parameters of Shen 2009 to their equation 29, predicted SMBH mass ($M_{\text{BH},\text{predicted}}$), after AGN phase, can be written as:

$$M_{\text{BH},\text{predicted}} = \frac{L_{\text{COSMOS}}}{3l_{\text{Edd}}} \left(1 - \frac{2\ln f}{3}\right), \quad (10)$$

and

$$f = \frac{3l_{\text{Edd}}M_{\text{BH},\text{initial}}}{L_{\text{COSMOS}}} \quad (11)$$

where $l_{\text{Edd}} = 1.26 \times 10^{38} \text{ ergs}^{-1} M_{\odot}^{-1}$.

Through Monte Carlo realisations we take into account: all possible seed values that could be assigned to the merging DMHs; all possible luminosities in each luminosity bin of Bongiorno et al. 2012; scatter in Ferrarese 2002 M_{BH} - M_{DMH} relation; scatter in Shen 2009 $M_{\text{BH},\text{final}}$ - $M_{\text{DMH},\text{post}}$ relation; and scatter in Rodriguez-Puebla et al. 2015 M_* - M_{DMH} relation. In the last mentioned scatter, same halo can host a galaxy below or above $\log(M_*/M_{\odot}) = 10.4$. As the result, depending on the random draw from the scatter in each Monte Carlo realisation, some halos might drop from the analysis while others might join.

At the end we have $M_{\text{BH},\text{final}}$ from our best fit model and in 40,000 Monte Carlo realisations we produce $M_{\text{BH},\text{predicted}}$ in each Δz - ΔM_* interval. Now we can compare these two masses. If the observed AGN luminosities are indeed the peak luminosities when most of the SMBH growth occurs, then the mass of the predicted SMBH should match the mass of the final SMBH. We calculate the percentage of realisations when this condition is met.

3 RESULTS

3.1 Best fit model

We apply Shen 2009 major merger driven AGN activity model to the merger trees in cosmological N-body simulation. There are some differences between Shen 2009 and our model.

While Shen 2009 assumes constant ratio of 10^{-3} between initial and peak BH mass, we seed DMHs with BH seeds and follow their evolution before AGN phase. Hence, BH mass right before AGN phase is not necessarily a constant fraction of the peak BH mass. Also, we calibrate final SMBH mass at redshift $z = 0$ to the local Ferrarese relation. In this manner, SMBH mass is overestimated at high redshift to accommodate for the late DMH evolution. In our model, super-Eddington accretion starts when galaxies merge while in Shen 2009 model same occurs when DMHs merge.

Our best fit model for the SMBH growth reproduces observed AGN luminosity function, SMBH mass function, duty cycle, and bias. Both M1 and M2 models can be considered as best fit models. M2 model provides a slightly better fit to the observations hence we show this match for M2 model only.

Figure 2 shows BH mass function at three redshifts $z = [2.00, 1.25, 0.75]$. Horizontal and vertical

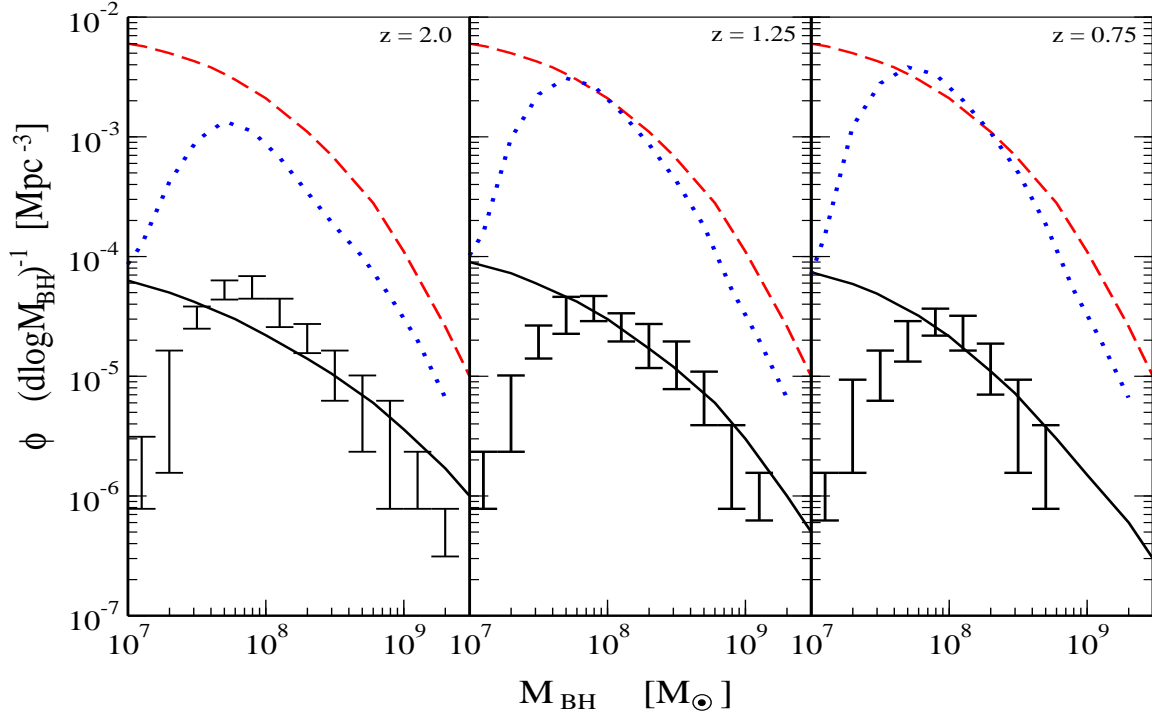


Figure 2. Black hole mass function at three redshifts $z = [2.00, 1.25, 0.75]$, for active black holes only, in AGNs with $\log L_X [\text{erg/s}] \geq 43$, where $X = [2 - 10]$ KeV. Horizontal and vertical bars show the full range of masses in our Monte Carlo realisations, for active black holes only, in AGNs with $\log L_X [\text{erg/s}] \geq 43$, where $X = [2 - 10]$ KeV. Dotted, blue line shows our BH mass function for all BHs. Overplotted as thick black line is active BH mass function for the same luminosity range from observations (HELLAS2XMM) of La Franca et al. 2005 (presented in Fiore et al. 2012). Also, in dashed red line is local BH mass function for all black holes (Merloni & Heinz 2008). Our best fit model is a good match to the observations.

bars show the full range for BH mass function, in our Monte Carlo realisations, for active black holes only, in AGNs with $\log L_X [\text{erg/s}] \geq 43$, where $X = [2 - 10]$ KeV. Dotted, blue line shows our BHs mass function for all BHs. Overplotted as thick black line is active BH mass function for the same luminosity range from observations (HELLAS2XMM) of La Franca et al. 2005 (presented in Fiore et al. 2012). Our best fit model follows the observed mass functions for active BHs. We slightly overestimate masses of active BHs at $z = 2$. This effect transfers to the lower redshift where our BH mass function for all BHs (dotted, blue) slightly overpredicts the local BH mass function at $\sim 10^8 M_\odot$ (dashed, red, Merloni & Heinz 2008). At larger BH masses our model underpredicts local BH mass function. We find that this occurs due to the arbitrary cut off at the higher mass end for halos capable of hosting AGNs. When this upper limit for halo mass is doubled, we get a perfect match to the local BH mass function for $M_{\text{BH}} > 10^8 M_\odot$. However, at the same time, we overpredict AGN luminosity function at $z < 1$ and $\log L_X [\text{erg/s}] > 44$ by a factor of 4. Similarly to Shen 2009, our model is incomplete at $M_{\text{BH}} \leq 10^{7.5} M_\odot$ because we did not include contri-

butions from AGNs triggered by secular processes or minor mergers.

Figure 3 shows AGN luminosity function with horizontal and vertical bars presenting the full range in our best fit model. Overplotted as thick black line is AGN luminosity function from same observations as in figure 2. Our best fit model deviates from the observations at $z = 2$ and $z = 0.75$. However, AGN luminosity functions reported in the literature deviate between various surveys. This can be seen when we overplot AGN luminosity function (dashed red line in Figure 3) from a large combination of X-ray surveys including XMM and Chandra COSMOS survey (Miyaji et al. 2015). Discrepancy between Fiore et al. 2012 and Miyaji et al. 2015 is comparable to the discrepancy between our best fit model and these observations.

Figure 4 shows AGN duty cycle as a function of stellar mass at three redshifts $z = [2.00, 1.25, 0.75]$. We consider AGNs with $\log L_X [\text{erg/s}] \geq 43$, where $X = [2 - 10]$ KeV. Horizontal and vertical bars show the full range for the duty cycle in our Monte Carlo realisations. Observations are again from La Franca et al. 2005 and Fiore et al. 2012. Our best fit model is a good match to the observations.

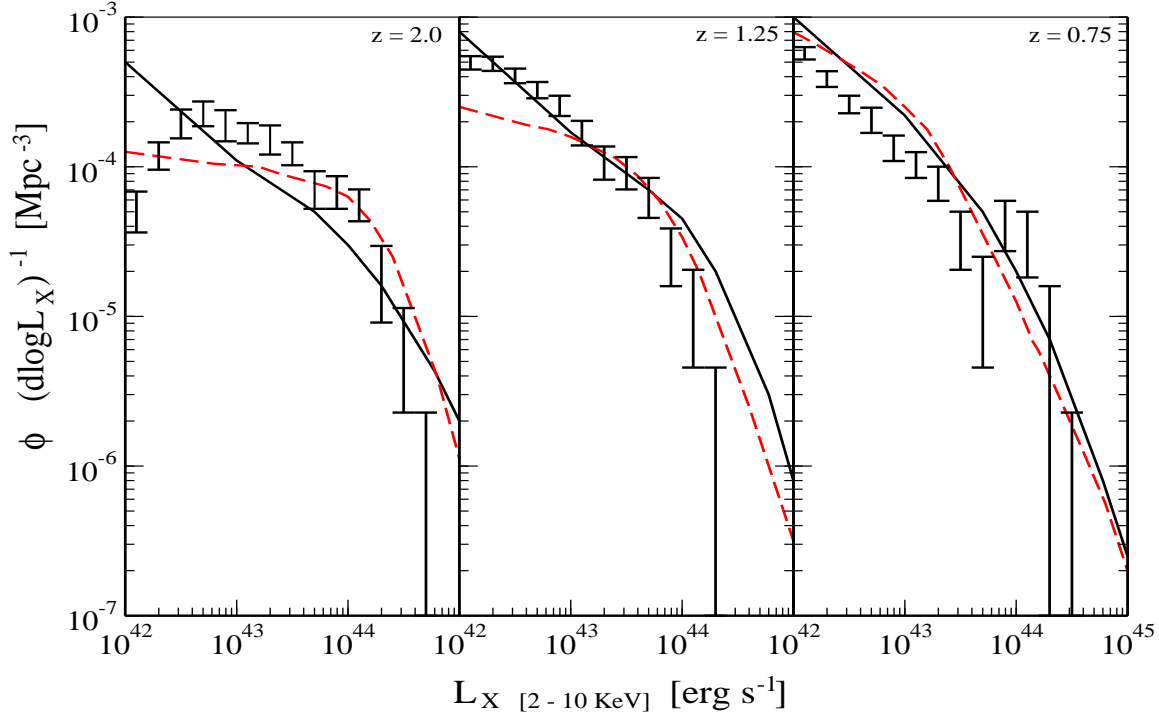


Figure 3. AGN luminosity function at three redshifts $z = [2.00, 1.25, 0.75]$. Horizontal and vertical bars present the full range in our best fit model. Overplotted as thick black line is AGN luminosity function from observations (HELLAS2XMM) of La Franca et al. 2005 (presented in Fiore et al. 2012). In dashed red line is AGN luminosity function from a large combination of X-ray surveys including XMM and Chandra COSMOS survey (Miyaji et al. 2015). Our best fit model is a good match to the observations although we slightly underpredict luminosity function toward lower redshifts.

Figure 5 shows AGN bias factor at three redshifts $z = [2.0, 1.5, 1.0]$. We have calculated AGN bias factor by using equations (3), (4), and (5) in Cappelluti, Allevato & Finoguenov 2012. From these equations, AGN bias in a luminosity and redshift range $\Delta L, \Delta z$ can be written as:

$$\text{bias}(\Delta L, \Delta z) = \frac{\Sigma b_{\text{DMH}}(\Delta L, \Delta z)}{N_{\text{AGN}}(\Delta L, \Delta z)}, \quad (12)$$

where $b_{\text{DMH}}(\Delta L, \Delta z)$ is the large scale bias of dark matter halos which host AGNs in the luminosity and redshift range $\Delta L, \Delta z$, and $N_{\text{AGN}}(\Delta L, \Delta z)$ is the total number of AGNs hosted by DMHs in the luminosity and redshift range $\Delta L, \Delta z$. We obtain b_{DMH} from figure 11 in Allevato et al. 2011.

Horizontal and vertical bars in figure 5 show the full range for AGN bias in our Monte Carlo realisations. Thick black line shows the best fit model in Shen 2009. Points are measurements from Croom et al. (2005, green-crosses), Porciani & Norberg (2006, green-star), Shen et al. (2009, green-open square), da Angela et al. (2008, green-circles), Myers et al. (2007, green-squares), and Allevato et al. 2011 (blue triangle). Red squares are from the semi analytic model of galaxy formation in Gatti et al. 2016. AGN bias

substantially differs from bias in Shen 2009 at low luminosities. This flattening could be induced by the Monte Carlo approach as it includes the broad scatterers in calculated parameters. Considering the uncertainties in determining AGN bias, our best fit model is a good match to the observations.

Figure 6 shows $M_{\text{BH}} - M_{\text{DMH}}$ relation in our best fit model. Red lines show full range of Monte Carlo realisations at redshift $z = 2$; blue lines represent the same at $z = 1$; and green lines at $z = 0$. Thick black line shows local Ferrarese relation at $z = 0$ and it matches our best fit model at $z = 0$ by the default since we calibrate our model to do exactly that. We find that this match occurs when $\sigma_{\text{sph}} = 0.77 \times V_{\text{vir}}$. Our model incorporates no evolution in $M_{\text{BH}} - \sigma_{\text{sph}}$ relation. It overpredicts BH mass at high redshift as BHs grow faster than DMHs. Figure 6 shows how $M_{\text{BH}} - M_{\text{DMH}}$ relation evolves into local Ferrarese relation as dark matter halos grow in mass and “catch up” to the BH growth.

Figure 7 shows $M_{\text{BH}} - M_{\star}$ relation in our best fit model (top panel). Horizontal and vertical bars show full range of Monte Carlo realisations at redshift $z = 0$. Black line shows Kormendy & Ho 2013 relation, and dashed green line shows Merloni & Heinz

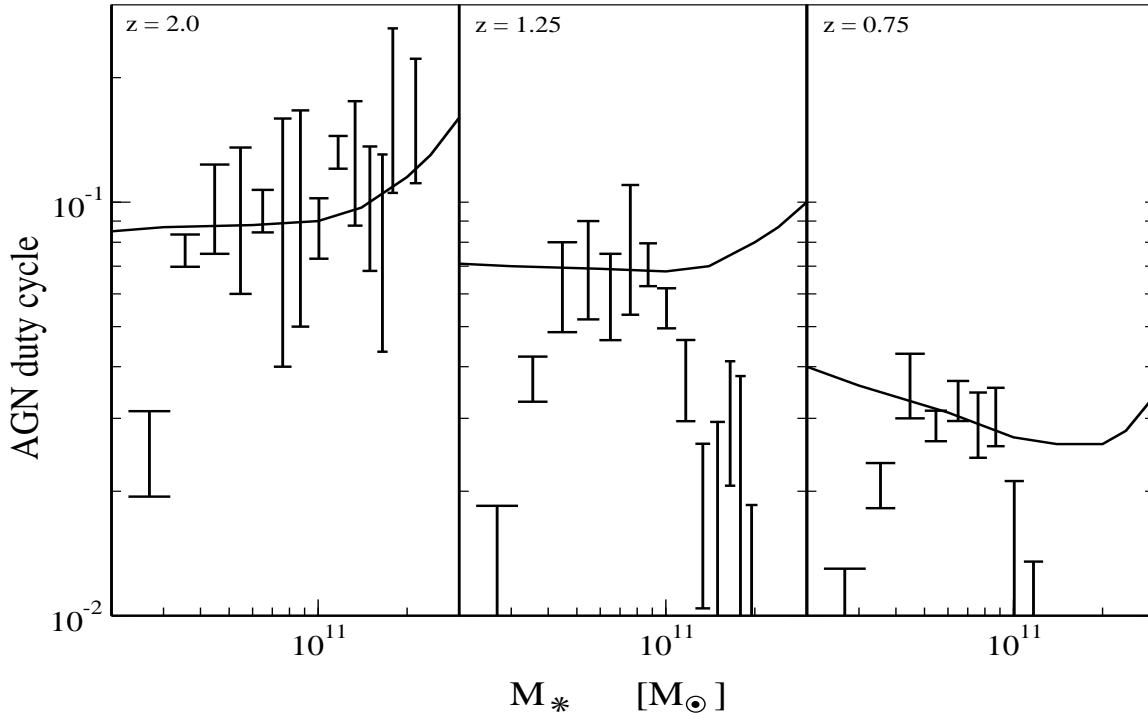


Figure 4. AGN duty cycle as a function of stellar mass at three redshifts $z = [2.00, 1.25, 0.75]$. We consider AGNs with $\log L_X [\text{erg/s}] \geq 43$, where $X = [2 - 10]$ KeV. Horizontal and vertical bars show the full range for duty cycle in our Monte Carlo realisations. Overplotted as thick black line is duty cycle for the same luminosity range from observations (HELLAS2XMM) of La Franca et al. 2005 (presented in Fiore et al. 2012). Our best fit model is a good match to the observations although we slightly underpredict duty cycle toward lower redshifts.

2008 relation. Our best fit model underpredicts BH masses when compared to Kormendy & Ho 2013 relation. However, the match is better when compared to Merloni & Heinz 2008 relation. We also find no evolution of scatter in $M_{\text{BH}} - M_*$ relation in our best fit model (bottom panel in figure 7). Despite the BH mass being determined by σ_{sph} via V_{vir} , and the scatter in M_* at fixed M_{DMH} is very small, the resulting $M_{\text{BH}} - M_*$ relation of figure 7 is very broad and even significantly below the Kormendy & Ho 2013 relation. This might be in support of the biases in the local scaling relations of BHs and galaxies discussed recently in the literature (Reines & Volonteri 2015, van den Bosch et al. 2015, Shankar et al. 2016, Greene et al. 2016, van den Bosch 2016).

3.2 Determining AGN activity phase

Assuming that major mergers are driving AGN activity in massive galaxies, we have selected simulated mergers of field galaxies in the redshift range $0.3 < z < 2.5$ and matched them to the observed samples of AGNs in redshift and galaxy-mass bins in F14.

Matching procedure briefly consists of: As halo merger finishes, galaxy merger starts. We define that

as a time of AGN peak activity corresponding to the AGN observed in COSMOS survey. The mass of simulated galaxy hosting the AGN is derived from halo-galaxy scaling relation.

Once we find redshift bin and galaxy-mass bin of the simulated merger, we trace the merging halos before the merger, and we trace merger remnant after the merger. We determine initial SMBH mass (before accretion during AGN phase) and final (“true”) SMBH mass (after accretion in AGN phase).

Figure 8 shows BHs mass function in model M1 (left panels) and M2 (right panels) for both initial BHs $M_{\text{BH,initial}}$ (thick, black line) and for the final BHs $M_{\text{BH,final}}$ (thin, red line), in the three redshift ranges: top panel: $0.3 < z < 0.8$; middle panel: $0.8 < z < 1.5$; bottom panel: $1.5 < z < 2.5$. Bars represent full range of Monte Carlo realisations which cover possible $M_{\text{BH,initial}}$ from log-normal distribution defined for massive seed BHs in spiral galaxies; scatter in Ferrarese 2002 $M_{\text{BH}} - M_{\text{DMH}}$ relation for BHs at the centres of elliptical galaxies; and scatter in Kormendy & Ho 2013 $M_{\text{BH}} - \sigma_{\text{sph}}$ relation for the final “true” BH mass in postmerger halos. It also covers (not that obvious) scatter in Rodriguez-Puebla et al. 2015 $M_* - M_{\text{DMH}}$ relation applied as a selection criterion for el-

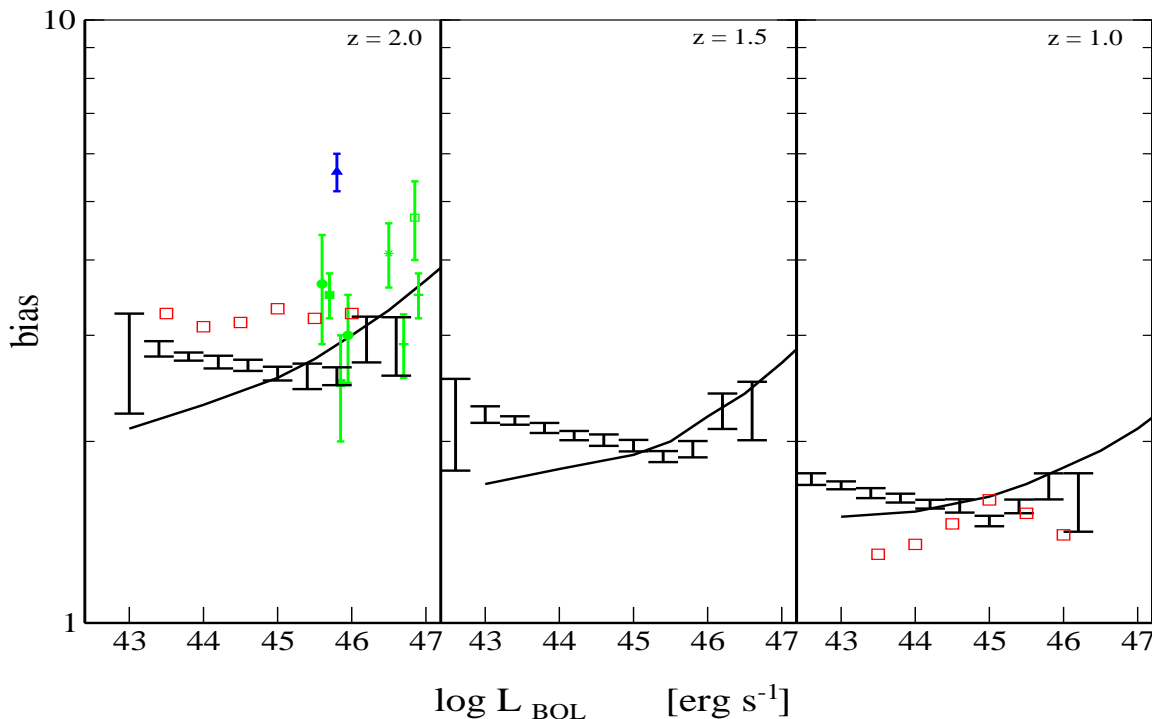


Figure 5. AGN bias factor at three redshifts $z = [2.0, 1.5, 1.0]$. Horizontal and vertical bars show the full range for AGN bias in our Monte Carlo realisations. Thick black line shows the best fit model in Shen 2009. Points are measurements from Croom et al. (2005, green-crosses), Porciani & Norberg (2006, green-star), Shen et al. (2009, green-open square), da Angela et al. (2008, green-circles), Myers et al. (2007, green-squares), and Allevato et al. 2011 (blue triangle). Red squares are from the semi analytic model of galaxy formation in Gatti et al. 2016. Considering the uncertainties in determining AGN bias, our best fit model is a good match to the observations.

lptical galaxies at z_{AGN} . Because of this scatter, same halo can host a galaxy below or above $\log(M_*/M_\odot) = 10.4$. As the result, depending on the random draw from the scatter in each Monte Carlo realisation, some halos might drop from the analysis while others might join.

Premerger accretion occurs between z_{initial} and z_{AGN} and it consists of two phases: first, the pre-BHB phase before initial BHs form binary; and second, BHB phase which lasts for ~ 100 Myr before BHs merge as BHs in the binary overcome last couple of kiloparsecs. The typical pre-BHB timescale for BHs in spiral galaxies is ~ 2 Gyr. Since accretion rate in model M1 is set to $10^{-4} M_\odot \text{yr}^{-1}$ the amount of mass accreted then during this phase is $\sim \text{few} \times 10^5 M_\odot$. During BHB phase BHs double their masses. After adding mass from both pre-BHB and BHB phases to the seed BHs in spiral galaxies their mass function peaks at $10^{5.5} M_\odot - 10^6 M_\odot$ depending on the redshift (figure 8, left panels). On the other hand, mass function of the initial BHs in the elliptic galaxies peaks at $10^{6.5} M_\odot - 10^7 M_\odot$ (figure 8, left panels).

In model M2, the pre-BHB accretion is set to $10^{-3} M_\odot \text{yr}^{-1}$ so the amount of mass accreted during

this phase is $\sim \text{few} \times 10^6 M_\odot$. After both pre-BHB and BHB phases, and after adding the accreted mass to the seed BHs in spiral galaxies, their masses overlap with the masses of BHs in elliptical galaxies. Resulting mass function peaks at $10^{6.5} M_\odot - 10^{6.9} M_\odot$ depending on the redshift (figure 8, right panels).

The difference in mass function between initial and final BHs in figure 8, is the accreted mass during AGN phase in our best fit model where L_{peak} is calculated from the light curve model in Shen 2009. M_{final} obtained in this manner (the “true” final BH mass) is then compared to $M_{\text{predicted}}$ which is obtained by replacing L_{peak} with AGN luminosities from COSMOS survey L_{COSMOS} .

All galaxies in the specific mass range, host AGNs with the probability defined in F14. Probability functions presented in F14 show that galaxies are more likely to host less luminous AGNs. As the observed AGN luminosity increases, the probability for that particular AGN to be observed in the COSMOS galaxy decreases. We incorporate COSMOS AGN luminosities into Shen 2009 model for SMBH growth.

We perform 40,000 Monte Carlo realisations for every M_{initial} in each $\Delta z - \Delta M_*$ interval, through all

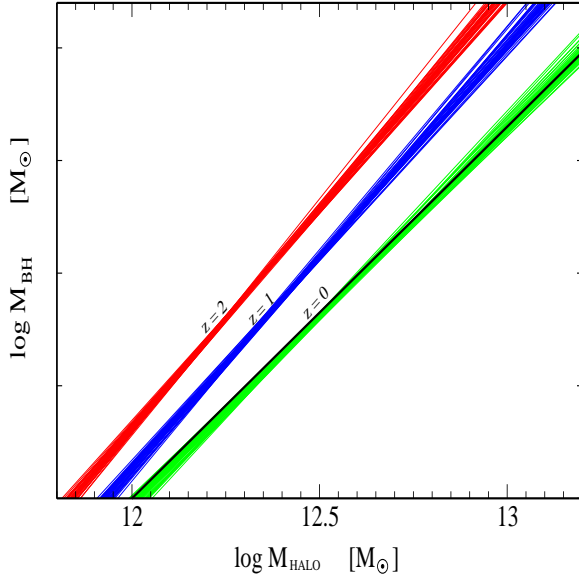


Figure 6. $M_{\text{BH}} - M_{\text{DMH}}$ relation in our best fit model. Red lines show full range of Monte Carlo realisations at redshift $z = 2$; blue lines represent $z = 1$; and green lines $z = 0$. Thick black line shows local Ferrarese relation at $z = 0$. Figure shows how $M_{\text{BH}} - M_{\text{DMH}}$ relation evolves into local Ferrarese relation as dark matter halos grow in mass.

possible COSMOS AGN luminosities. As the result, we obtain 40,000 predicted BH masses which we compare to the “true” final BH mass. When $M_{\text{predicted}} \geq M_{\text{final}}$, COSMOS AGN luminosity is the peak AGN luminosity, corresponding to the AGN luminosity in our best fit model. We calculate the percentage of realisations where $M_{\text{predicted}}$ is at least as large as M_{final} and present it in figure 9.

Figure 9 shows the probability function (occupation fraction) that the observed AGNs are at their peak activity. Nine panels present three redshift ranges and three galaxy log-mass ranges. Thick (black) bars represent probability functions in our model M1. Thin (red) bars represent probability functions in our model M2. Bars show full range of Monte Carlo realisations. Probability for peak AGN activity at low redshift $z=[0.3, 0.8]$ is small in all galaxy mass bins. For $M_* = [10.4, 10.7]$ all AGNs have probability $< 20\%$ in model M1, and $< 30\%$ in model M2. In the same $\Delta z - \Delta M_*$ interval, probability of $< 10\%$ have 90 - 100 % of AGNs in M1 and 80 - 90 % of AGNs in M2. The occupation fraction of AGNs with low probability for peak activity increases toward larger galaxy mass. AGNs hosted by most massive galaxies ($M_* = [10.9, 11.2]$) are all in the declining phase of their activity since probability drops to $< 20\%$ in both models (top, right panel in figure 9). Overall, at low redshift, almost all AGNs are in non-star-forming Red Sequence galaxies.

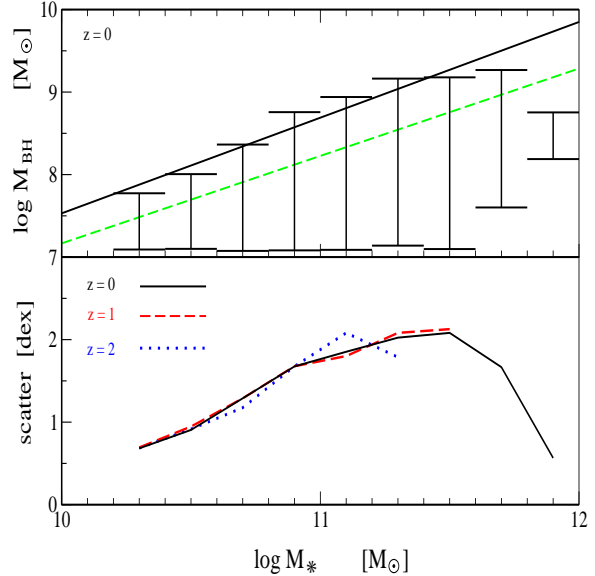


Figure 7. Top panel: $M_{\text{BH}} - M_*$ relation in our best fit model. Horizontal and vertical bars show full range of Monte Carlo realisations at redshift $z = 0$. Black line shows Kormendy & Ho 2013 relation, and dashed green line shows Merloni & Heinz 2008 relation. Bottom panel: evolution of scatter in $M_{\text{BH}} - M_*$ relation in our best fit model (dotted blue line for $z = 2$; dashed red line for $z = 1$; and thick black line for $z=0$).

Increase in fraction of AGNs with larger probability means more AGNs are in star forming Green Valley galaxies. We see this trend as we go from low to high redshift in figure 9. At the intermediate redshifts ($z=[0.8, 1.5]$) AGN fraction with larger probability increases in both models (middle panels in Figure 9). As expected, this increase is larger for M2 where $M_{\text{BH,initial}}$ is larger. Still, most AGNs have low probability for being observed at their peak. AGNs at high redshifts ($z=[1.5, 2.5]$), and in the lowest galaxy mass range ($M_* = [10.4, 10.7]$, bottom, left panel in figure 9) are dominantly at the peak activity since 30 - 50 % of them in M1 and 55 - 75 % in M2 have $> 80\%$ probability for being at the peak. Overall, distribution of occupation fractions shifts toward larger probabilities. Similarly to lower redshifts, occupation fraction with large probabilities decreases toward more massive galaxies. For $M_* = [10.7, 10.9]$ (bottom, middle panel in figure 9), AGN fraction is evenly distributed. Here we would expect to see comparable numbers of AGNs in both quiescent and star forming galaxies. In the largest mass range (panels on the right of Figure 9) AGNs are predominantly in quiescent galaxies at all redshifts.

So the trend that emerges in figure 9 is that quiescent galaxies host almost all AGNs at low redshift. As we go toward higher redshift there are more AGNs

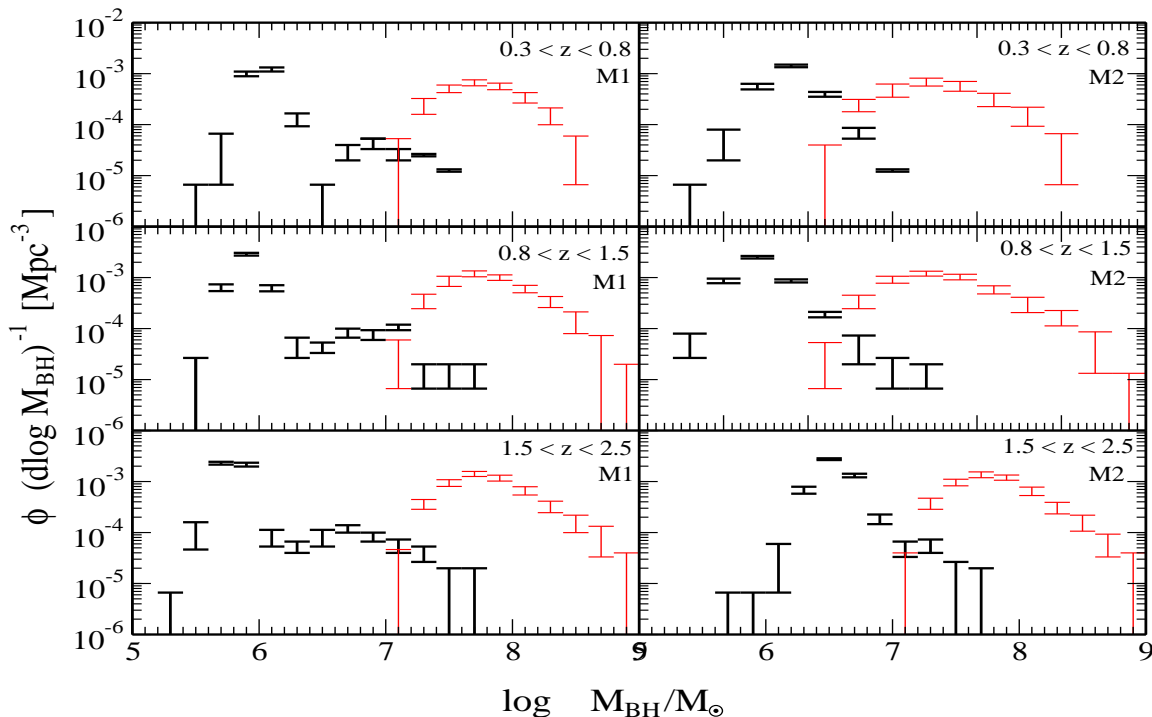


Figure 8. BH mass function for model M1 with bars representing full range of Monte Carlo realisations. $M_{\text{BH,initial}}$ represented in thick, black. $M_{\text{BH,final}}$ represented in thin, red. Three redshift ranges: top panel: $0.3 < z < 0.8$; middle panel: $0.8 < z < 1.5$; bottom panel: $1.5 < z < 2.5$. BH mass function for model M2.

in star forming galaxies and the percentages of AGNs inhabiting quiescent galaxies and star forming galaxies become comparable. We also see the trend with increasing galaxy mass. At larger galaxy masses there are more AGNs in quiescent galaxies.

This exact trend we see in AGNs in COSMOS survey (Figures 12, 13 and 18, Bongiorno et al. 2012).

4 DISCUSSION AND CONCLUSIONS

We ran cosmological (130 Mpc box) N-body (dark matter only) simulation from which we located field DMHs at all redshifts. We also followed their evolution while they stay in the field. We found merger events and traced merger progenitors and merger remnants. Through scaling relations we calculated SMBH masses for progenitors and remnants. In this manner we obtain the SMBH mass at the centres of DMHs before (initial SMBH) and after (final SMBH) the merger.

We assume that at the time when halo merger finishes, galaxy merger starts. At that time newly formed SMBH ignites as AGN and quickly reaches its peak activity. We focus on two models with different range for the initial BH mass since BH seeds in spiral galaxies and their pre-coalescence growth are the source of largest uncertainty in our modelling. Model M1 has a

lower mass range $\sim [10^5 - 10^6] M_{\odot}$ and pre-coalescence accretion rate of $10^{-4} M_{\odot} \text{yr}^{-1}$. Model M2 has a larger initial mass range $\sim [10^{5.5} - 10^{6.5}] M_{\odot}$ and accretion rate of $10^{-3} M_{\odot} \text{yr}^{-1}$.

We determine “true” final BH mass by using non-evolving $M_{\text{BH}} - \sigma_{\text{sph}}$ relation where $\sigma_{\text{sph}} = 0.77 \times V_{\text{vir}}$. In this manner, $M_{\text{DMH}} - M_{\text{BH}}$ relation evolves from overestimating BHs masses at high redshift to matching local Ferrarese relation at $z=0$.

Our best fit model for the SMBH growth reproduces observed AGN luminosity function, SMBH mass function, duty cycle and bias.

Next, we replace peak AGN luminosities in our best fit model with COSMOS AGN luminosities from Bongiorno et al. 2012.

For every galaxy hosting an AGN we determine redshift and mass, and sort them into redshift ranges and mass ranges as in Bongiorno et al. 2012, COSMOS survey. For each mass and redshift, we assign an observed probability function for a galaxy to host an AGN of a certain luminosity (Figure 14 in Bongiorno et al. 2012). Next we ran 40,000 Monte Carlo realisations in each $\Delta z - \Delta M_{\star}$ interval where we draw from the observed probability functions and we assign luminosities to the initial BH. We obtain 40,000 predicted BH masses which we compare to the “true” final BH mass.

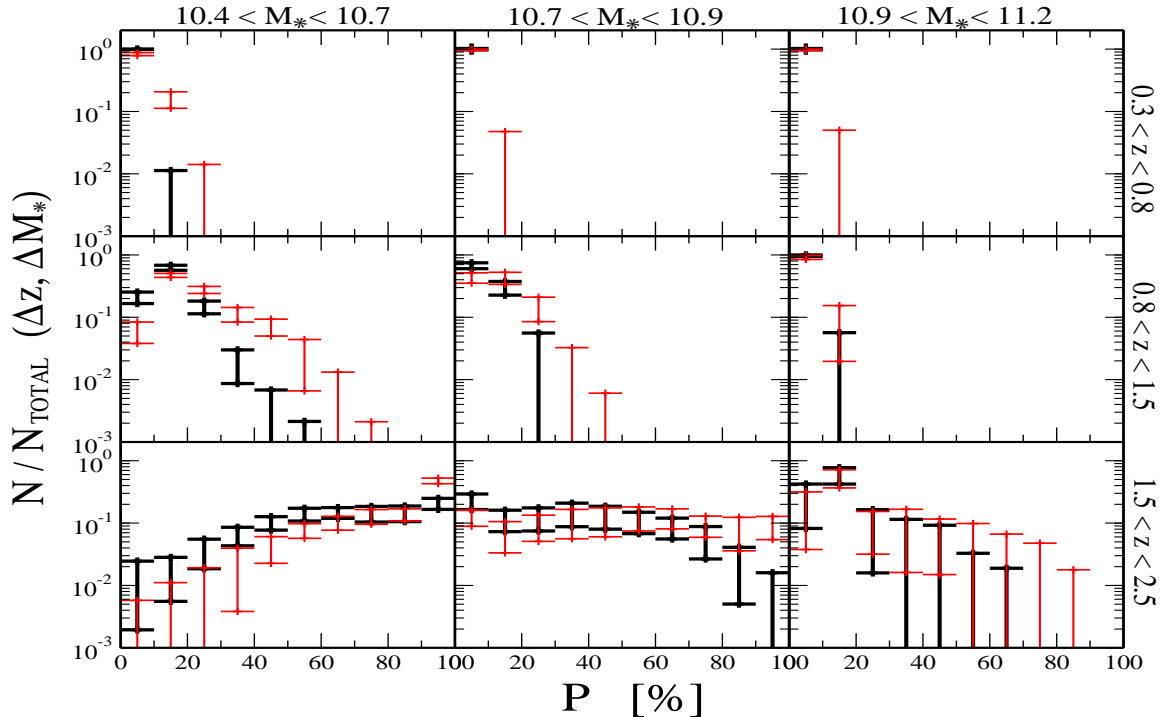


Figure 9. Probability function for the predicted SMBH mass to be at least as large as the true SMBH mass. In other words, probability that the observed AGN luminosity is large enough to account for the final SMBH mass. Probability functions are split into redshift bins and galaxy mass bins which correspond to nomenclature in Bongiorno et al. 2012. Thick (black) histograms represent probability functions in our model M1. Thin (red) histograms represent probability functions in our model M2.

When $M_{\text{predicted}} \geq M_{\text{final}}$, COSMOS AGN luminosity is the peak AGN luminosity, corresponding to the peak AGN luminosity in our best fit model. We calculate the percentage of realisations where $M_{\text{predicted}}$ is at least as large as M_{final} . Large percentage implies large probability for AGNs to be at their peak activity. Small percentage means that AGNs are not observed at the peak but in the declining phase of their nuclear activity. In this manner, we distinguish “peak” AGNs (recently merger triggered and hosted by star forming galaxies, Green Valley) and “faded” AGNs (merger triggered a long time ago and now residing in quiescent galaxies, Red Sequence).

At low redshift range ($z=[0.3, 0.8]$) all observed AGNs are in the declining phase of their nuclear activity, fading away (figure 9). The probability for being at their peak activity is $< 10\%$ for $> 90\%$ of AGNs in the most massive galaxies. AGN luminosity would have to be very large to account for the SMBH growth. But even if this highest possible luminosity was large enough to produce final SMBH, it is also the least probable one. Since the entire range of luminosities can not produce final SMBH, then these luminosities do not correspond to the AGN peak activity. The time of maximum nuclear activity when

most of the mass was accreted has occurred in the past at higher Eddington ratio when AGN luminosity was larger and when AGN was most likely hosted by star-forming galaxy (Green Valley). Logical conclusion is that the observed luminosities belong to the AGN in the declining phase of its nuclear activity which places this particular AGN in the quiescent galaxy (Red Sequence).

Theoretical modelling of AGN populations in hosts of various morphologies, mass ranges and redshifts, support the merger driven scenario for luminous AGN activity. At the same time observations are split between existence of merger features (Schawinski et al. 2010, Smirnova, Moiseev & Afanasiev 2010, Koss et al. 2010, Cotini et al. 2013) and the lack of them (Gabor et al. 2009, Darg et al. 2010, Cisternas et al. 2011, Kocevski et al. 2012, Villforth et al. 2014). Villforth et al. 2014 found no increase in the prevalence of merger signatures with AGN luminosity (in the redshift range $z = [0.5, 0.8]$) and concluded that major mergers either play only a very minor role in the triggering of AGN in the luminosity range studied ($\log L_x = [41, 44.5]$) or time delays are too long for merger features to remain visible.

Our model shows that the merger driven scenario

is still consistent with the observations even though there are no merger features in massive galaxies hosting low redshift AGNs and almost all of the AGN hosts are quiescent galaxies. How can mergers explain AGN activity in massive galaxies which have no merger features and no star formation to indicate recent galaxy merger? Since at $z = [0.3, 0.8]$ (figure 9) the observed luminosities can not correspond to AGNs at their peak activity (can not produce final SMBH mass in the simulation), then they must be observed much later in their evolution long after the merger features can be detected. And our confirmation of Bongiorno et al. 2012 results that almost all low redshift AGNs are in quiescent galaxies is a simple consequence of the drop in galaxy merger rates at $z < 1$. Since galaxy merger rates fall dramatically at low redshift, there are very few recently activated AGNs which would be hosted by star forming galaxies. So most of the observed AGNs are the fading AGNs activated in the old mergers which occurred at higher redshifts. Since there are no new galaxy mergers, almost all observed AGNs are in non-star-forming galaxies.

As we go toward higher redshifts, the probability for the AGNs being at their peak activity increases. There are more AGNs in star-forming Green Valley galaxies. At $z=[1.5, 2.5]$ the percentage of AGNs in star forming galaxies is comparable to the percentage of AGNs in quiescent galaxies. This can be seen in our figure 9, bottom panels, and in Figure 18 of Bongiorno et al. 2012. Again, this is a simple consequence of the large merger rate in galaxies at high redshift. The explanation for comparable number of star forming and quiescent AGN hosts is that AGNs in star forming galaxies at high redshift have “just” been triggered by galaxy mergers while AGNs in quiescent galaxies at the same redshift have been merger triggered at some time in the past.

Schawinski et al. 2014 had proposed a split of Green Valley transition into two paths. Current understanding is that late type galaxies transition slowly from Blue Cloud to Red Sequence, while hosting low to intermediate luminosity AGNs driven by secular processes. Early type galaxies transition fast, while hosting high luminosity AGNs driven by major mergers. In the context of galaxy evolution, our model addresses the evolution of early type galaxies which are produced in major mergers of gas-rich disk/spirals. These galaxies correspond to the massive, red galaxies in COSMOS survey (Bongiorno et al. 2012) where they represent the majority of AGN hosting galaxies. According to our model, AGNs in massive galaxies of the COSMOS survey, belong to the rapid transition channel (Schawinski et al. 2014). We find that, right after the merger, AGNs reach their peak activity (Green Valley phase). This is a short phase (~ 100 Myr) during which star formation is quenched. Then, galaxies enter Red Sequence phase with AGNs in the decline (or at the end) of their nuclear activity and low Eddington accretion rate observed in COSMOS sur-

vey. Figure 2 shows that we are sampling the growth of SMBHs $> 10^7 M_\odot$. For the most part, final SMBHs are $> 10^8 M_\odot$. This is consistent with Hopkins, Kocevski & Bundy 2014 conclusion that at these masses merger driven AGN activity dominates.

There are a number of recent papers discussing possible biases in the local scaling relations of BHs and galaxies (Reines & Volonteri 2015, van den Bosch et al. 2015, Shankar et al. 2016, Greene et al. 2016, van den Bosch 2016). In support of this, we find that when σ_{sph} is determined via V_{vir} , the resulting $M_{\text{BH}} - M_*$ relation of figure 7 is very broad and even significantly below the Kormendy & Ho 2013 relation. Shankar et al. 2016 found that the normalisation of the $M_{\text{BH}} - \sigma$ relation might be decreased by a factor of 3. Revising $M_{\text{BH}} - \sigma$ relation in our best fit model leads to smaller final BH masses. This in turn decreases BH mass functions and AGN luminosity functions by a similar factor but still consistent with the observations. We have tested how this fact would influence our results and we found that the probability functions in figure 9 would shift toward higher probabilities but would not qualitatively change our results.

We conclude that merger driven scenario for AGN activity is consistent with the observations and that the occupation fractions of the observed AGNs simply follow the evolution of galaxy merger rates. Our model reproduces the observed trend that quiescent (Red Sequence) galaxies host almost all AGNs at low redshift due to the dramatic drop in galaxy merger rates at $z < 1$. There are just few recently activated AGNs in star forming galaxies. Instead, most AGNs are in their declining nuclear activity hosted by quiescent galaxies. As we go toward higher redshift ($z > 1$), galaxy merger rates increase, and there are more peak activity AGNs observed in star forming galaxies. The percentage of peak AGNs inhabiting star forming and the percentage of faded AGNs hosted by quiescent galaxies becomes comparable. We also confirm the observed trend with increasing galaxy mass. At larger galaxy masses there are more AGNs in quiescent galaxies.

Our method for matching simulated DMH merger events with observations of field AGNs will be more accurate as the statistics improves with the future surveys. At this point, limited statistics of the sample prevents more detailed investigations of the incidence of AGN in galaxies as a function of redshift, stellar mass, star-formation rate and nuclear luminosity (Bongiorno et al. 2012). Wide area surveys will be necessary to probe volumes at $z > 1$ comparable to that explored by SDSS. At the low end of the galaxy mass distribution $\log [10.4, 10.7] M_\odot$, and high redshift $[1.5, 2.5]$, the probability functions in Bongiorno et al. 2012 do not have AGNs with $\log L_X [\text{erg/s}] \leq 44$. Most likely missed in COSMOS survey, since there are AGNs in this luminosity and galaxy mass range at lower redshifts. Including lower luminosities would change probability functions in Figure 14 of Bongiorno

et al. 2012, and would most likely shift AGN occupation fractions toward lower probabilities.

Even though we enforce criterion on AGN hosts to be $> 10^{10.4} M_{\odot}$ in stellar mass, we must have some mixing of populations. We expect that a large majority of AGNs in these galaxies are merger driven. However, some percentage of AGNs is probably driven by secular processes. That being said, we would like to point out that we are not trying to show that mergers are definitely responsible for AGN activity. We are arguing that observed AGN activity (at least in $> 10^{10.4} M_{\odot}$ galaxies) is consistent with mergers as drivers. However, this does not exclude other mechanisms. In fact, one could imagine a scenario where all of the moderate to faint AGNs are secularly driven.

Two major concerns for our method are: precision in determining the mass of the AGN host galaxy in observations, and detecting low luminosity AGNs. Both concerns impact the relations between mass of the host galaxy and probability functions for AGN incidence.

ACKNOWLEDGMENTS

Authors would like to thank the anonymous reviewer for the tremendous help with shaping this paper.

This work was supported by the Ministry of Education, Science and Technological Development of the Republic of Serbia through project no. 176021, “Visible and Invisible Matter in Nearby Galaxies: Theory and Observations”. The author acknowledges the financial support provided by the European Commission through project BELISSIMA (BELgrade Initiative for Space Science, Instrumentation and Modelling in Astrophysics, call FP7-REGPOT-2010-5, contract no. 256772).

Numerical results were obtained on the PARADOX cluster at the Scientific Computing Laboratory of the Institute of Physics Belgrade, supported in part by the national research project ON171017, funded by the Serbian Ministry of Education, Science and Technological Development.

REFERENCES

- Allevato, V., et al., 2011, *ApJ*, 736, 99
 Barnes, J. E., Hernquist, L. E., 1996, *ApJ*, 471, 115
 Barnes, J. E., 1988, *ApJ*, 331, 699
 Begelman, M. C., Volonteri, M., Rees, M. J., 2006, *MNRAS*, 370, 289
 Begelman, M. C., Rossi, E. M., Armitage, P. J., 2008, *MNRAS*, 387, 1649
 Behroozi, P. S., Wechsler, R. H., Wu, H. Yi., 2013, *ApJ*, 762, 109B
 Behroozi, P. S., Wechsler, R. H., Wu, H. Yi, Busha, M. T., Klypin, A. A., Primack, J. R., 2013, *ApJ*, 763, 18
 Binney, J., Tremaine, S., 1987, *Galactic Dynamics* (Princeton: Princeton Univ. Press)
 Bohm, A., Wisotzki, L., & GEMS team 2007, *ASP Conf. Ser.* 379, Metcalfe, N. & Shanks, T. (eds.), 185
 Bohm, A., et al., 2013, *A&A*, 549A, 46
 Bongiorno, A., et al., 2012, *MNRAS*, 427, 3103B
 Bromm, V., Loeb, A., 2003, *ApJ*, 596, 34
 Cales, S. L., et al. 2013, *ApJ*, 762, 90
 Canalizo, G., Stockton, A., 2000, *AJ*, 120, 1750
 Canalizo, G., Stockton, A., 2001, *ApJ*, 555, 719
 Cao, X., 2010, *ApJ*, 725, 388
 Capelo, P. R., Volonteri, M., Dotti, M., Bellovary, J. M., Mayer, L., Governato, F., 2015, *MNRAS*, 447, 2123C
 Cappelluti, N., Allevato, V., Finoguenov, A., 2012, *AdAst*2012E, 55
 Cavaliere, A., Vittorini, V., 2000, *ApJ*, 543, 599
 Cen, R., 2012, *ApJ*, 755, 28
 Ciotti, L., Ostriker, J. P., 2007, *ApJ*, 665, 1038
 Ciotti, L., Ostriker, J.P., Proga, D., 2010, *ApJ*, 717, 708
 Cisternas, M. et al., 2011, *ApJ*, 726, 57
 Cotini, S., Ripamonti, E., Caccianiga, A., Colpi, M., Della Ceca, R., Mapelli, M., Severgnini, P., Segreto, A., 2013, *MNRAS*, 431, 2661
 Crocce, M., Pueblas, S., Scoccimarro, R., 2006, *MNRAS*, 373, 369
 Croom, S. M., et al., 2005, *MNRAS*, 356, 415
 Croton, D. J., et al., 2006, *MNRAS*, 365, 11
 da Angela, J., et al. 2008, *MNRAS*, 383, 565
 Darg, D. W., et al., 2010, *MNRAS*, 401, 1552
 Dressler, A., 1980, *ApJ*, 236, 351
 Ellison, S.L., Patton, D.R., Mendel, J.T., Scudder, J.M., 2011, *MNRAS*, 418, 2043
 Ellison, S. L., Mendel, J. T., Patton, D. R., Scudder, J. M., 2013, *MNRAS*, 435, 3627
 Ferrarese, L., 2002, *ApJ*, 578, 90
 Fiore, F., et al., 2012, *A&A*, 537A, 16
 Gabor, J. M., et al., 2009, *ApJ*, 691, 705
 Gaskell, C. M., 2009, *arXiv*0908.0328G
 Gatti, M., Shankar, F., Bouillot, V., Menci, N., Lamas, A., Hirschmann, M., Fiore, F., 2016, *MNRAS*, 456, 1073
 Gerhard, O. E., 1981, *MNRAS*, 197, 179
 Greene, J. E., et al., 2016, *arXiv*160600018
 Hayward C. C., Torrey P., Springel V., Hernquist L., Vogelsberger M., 2014, *MNRAS*, 442, 1992
 Hernquist, L., 1989, *Nature*, 340, 687
 Hopkins, P. F., Hernquist, L., Cox, T. J., Robertson, B., Di Matteo, T., Springel, V., 2006, *ApJ*, 639, 700
 Hopkins, P. F., Richards, G. T., Hernquist, L., 2007, *ApJ*, 654, 731H
 Hopkins, P. F., Hernquist, L., Cox, T. J., Keres, D., 2008, *ApJS*, 175, 356
 Hopkins, P.F., 2012, *MNRAS*, 420, L8
 Hopkins, P. F., Kocevski, D. D., Bundy, K., 2014, *MNRAS*, 445, 823H
 Hwang, H. S., Park, C., Elbaz, D., Choi, Y. Y., 2012, *A&A*, 538, 15
 Kocevski, D. D., et al., 2012, *ApJ*, 744, 148
 Komatsu, E., et al., 2009, *ApJS*, 180, 330
 Kormendy, J., Ho, L. C., 2013, *ARA&A*, 51, 511
 Kormendy, J., Kennicutt, Jr., R. C., 2004, *ARA&A*, 42, 603
 Koss, M., Mushotzky, R., Veilleux, S., Winter, L., 2010, *ApJ*, 716, 125
 La Franca, F., et al., 2005, *ApJ*, 635, 864
 Lake, G., Katz, N., Moore, B., 1998, *ApJ*, 495, 152

- Lapi, A., Shankar, F., Mao, J., Granato, G. L., Silva, L., De Zotti, G., Danese, L., 2006, *ApJ*, 650, 42
- Li, Y.-R., Ho, L. C., Wang, J.-M., 2011, *ApJ*, 742, 33
- Martini, P., Sivakoff, G. R., Mulchaey, J. S., 2009, *ApJ*, 701, 66
- Menci, N., et al., 2004, *ApJ*, 604, 12
- Menci, N., et al., 2008, *ApJ*, 647, 753
- Merloni, A., Heinz, S., 2008, *MNRAS*, 388, 1011
- Miyaji, T., et al., 2015, *ApJ*, 804, 104
- Mortlock et al., 2011, *Nature*, 474, 616
- Myers, A. D., et al. 2007, *ApJ*, 658, 99
- Naab, T., Jesseit, R., Burkert, A., 2006, *MNRAS*, 372, 839
- Negroponte, J., White, S. D. M., 1983, *MNRAS*, 205, 1009
- Novak, G. S., Jonsson, P., Primack, J. R., Cox, T. J., Dekel, A., 2012, *MNRAS*, 424, 635
- Porciani, C., Norberg, P., 2006, *MNRAS*, 371, 1824
- Rafferty, D. A., et al., 2011, *ApJ*, 742, 3
- Reines, A. E., Volonteri, M., 2015, *ApJ*, 813, 82
- Rodriguez-Puebla, A., Avila-Reese, V., Yang, X., Foucaud, S., Drory, N., Jing, Y. P., 2015, *ApJ*, 799, 130
- Roskar, R., Fiacconi, D., Mayer, L., Kazantzidis, S., Quinn, T. R., Wadsley, J., 2015, *MNRAS*, 449, 494
- Salpeter, E. E., 1964, *ApJ*, 140, 79
- Salviander, S., Shields, G. A., Bonning, E. W., 2015, *ApJ*, 799, 173
- Sanchez, S.F., et al., 2004, *ApJ*, 614, 586
- Sanders, D. B., Soifer, B. T., Elias, J. H., Madore, B. F., Matthews, K., Neugebauer, G., Scoville, N. Z., 1988, *ApJ*, 325, 74
- Schawinski, K., et al., 2007, *MNRAS*, 382, 1415
- Schawinski, K., Dowlin, N., Thomas, D., Urry, C. M., Edmondson, E., 2010, *ApJ*, 714, 108
- Schawinski, K., Treister, E., Urry, C.M., Cardamone, C.N., Simmons, B., Sukyoung, K., 2011, *ApJ*, 727, 31
- Schawinski, K., et al., 2014, *MNRAS*, 440, 889
- Shankar, F., Weinberg, D. H., Miralda-Escude, J., 2009, *ApJ*, 690, 20
- Shankar, F., et al., 2016, *MNRAS*, tmp, 465
- Shen, Y., et al. 2009, *ApJ*, 697, 1656
- Shen, Y., et al. 2015, *ApJ*, 805, 96
- Shankar, F., Bernardi, M., Haiman, Z., 2009, *ApJ*, 694, 867
- Shen, Y., 2009, *ApJ*, 704, 89
- Silverman, J.D., et al., 2008, *ApJ*, 675, 1025
- Silverman, J.D., et al., 2011, *ApJ*, 743, 2
- Simmons, B. D., Urry, C. M., Schawinski, K., Cardamone, C., Glikman, E., 2012, *ApJ*, 761, 75
- Smirnova, A. A., Moiseev, A. V., Afanasiev, V. L., 2010, *MNRAS*, 408, 400
- Springel, V., Yoshida, N., White, S. D. M., 2001, *NewA*, 6, 79S
- Springel, V. et al., 2005, *Nature*, 435, 629
- Surace, J. A., Sanders, D. B., 1999, *ApJ*, 512, 162
- Surace, J. A., Sanders, D. B., Evans, A. S., 2000, *ApJ*, 529, 170
- Tamburello, V., Capelo, P. R., Mayer, L., Bellovary, J. M., Wadsley, J., arXiv160300021T
- Toomre, A. 1977, in *Evolution of Galaxies and Stellar Populations*, ed. B. M. Tinsley & R. B. G. Larson, D. Campbell, 401
- van den Bosch, R. C. E., Gebhardt, K., Gultekin, K., Yildirim, A., Walsh, J. L., 2015, *ApJS*, 218, 10
- van den Bosch, R. C. E., Greene, J. E., Braatz, J. A., Constantin, A., Kuo, C. Y., 2016, *ApJ*, 819, 11
- Verdes-Montenegro, L., Sulentic, J., Lisenfeld, U., Leon, S., Espada, D., Garcia, E., Sabater, J. and Verley, S., 2005, *A&A*, 436, 443.
- Villforth, C., et al., 2014, *MNRAS*, 439, 3342
- Volonteri, M., Begelman, M. C., 2010, *MNRAS*, 409, 1022
- White, S. D. M., 1978, *MNRAS*, 184, 185
- White, S. D. M., 1979, *ApJ*, 229, L9
- Yu, Q., Lu, Y., 2008, *ApJ*, 689, 732